

Structural and electronic properties of the first iridium containing mixed B-site spinel oxide: $\text{Cu}[\text{Ir}_{1.5}\text{Cu}_{0.5}]\text{O}_4$

M. K. Wallace ¹, Jun Li ¹, P. G. Labarre,² S. Svdlenak ¹, D. Haskel,³ J. Kim ³, G. E. Sterbinsky,³ F. Rodolakis ³, H. Park,^{4,5} A. P. Ramirez,² and M. A. Subramanian ^{1,*}

¹Department of Chemistry, Oregon State University, Corvallis, Oregon 97331, USA

²Department of Physics, University of California Santa Cruz, Santa Cruz, California 95064, USA

³Advanced Photon Source, Argonne National Laboratory, Argonne, Illinois, 60439, USA

⁴Department of Physics, University of Illinois at Chicago, Chicago, Illinois 60607, USA

⁵Material Science Division, Argonne National Laboratory, Lemont, Illinois 60439, USA



(Received 20 April 2021; accepted 9 September 2021; published 27 September 2021)

Geometrically frustrated systems populated with large spin-orbit coupled ions are an ideal setting for the exploration of novel exotic states of matter. Here we present an example of iridium on a mixed B-site spinel oxide structure: $\text{Cu}[\text{Ir}_{1.498(2)}\text{Cu}_{0.502(2)}]\text{O}_4$. Synchrotron XRD refinements reveal a face-centered-cubic structure with space group $Fd\bar{3}m$ and mixed Cu-Ir site disorder within the B_2O_4 rocksalt substructure. Electrical properties reveal a metallic state within the 50–600-K range with a Kondo effect at $T < 50$ K. X-ray absorption spectroscopy (XAS) measurements show a mixed $\text{Cu}^{1+/2+}$ and $\text{Ir}^{3+/4+}$ charge partitioned picture, which suggests a metallic/band description with reduced on-site Coulomb interactions. Spin-glass-like freezing is seen at $T_g = 49$ K, and the hysteresis behavior for $T > T_g$ resembles that of a strongly frustrated magnet. DFT calculations show sizable hybridization between the Cu 3d and Ir 5d states with an effective mixed $\text{Ir}^{3+/4+}$ charge partitioned picture, supporting the electronic and XAS results.

DOI: [10.1103/PhysRevMaterials.5.094410](https://doi.org/10.1103/PhysRevMaterials.5.094410)

I. INTRODUCTION

Among the known varieties of geometrically frustrated frameworks, the AB_2X_4 spinel structure has been extensively investigated in the condensed matter physics community starting with Anderson's discussion of the spinel and inverse spinel structures [1]. The spinel structure consists of two basic units: AX_4 tetrahedron and BX_6 octahedron. The B_2X_4 network forms a rocksalt structure where alternate octahedral sites are occupied by the B cations (1/2 of the octahedral sites are occupied). The A cations occupy 1/8 of the tetrahedral sites; only tetrahedral sites with all four neighboring empty octahedral sites are filled. A unique feature of the spinel structure is that the B ions form a sublattice of corner-shared tetrahedra and the A ions form a diamond sublattice (Fig. 1). The B sublattice gives rise to strong magnetic frustration. Compounds with the AB_2X_4 spinel structure have provided fascinating insights in terms of their unusual properties due in part to geometrical frustration. Most spinel oxides, however, are known to be insulating. Only two spinel oxides, LiV_2O_4 and LiTi_2O_4 , are reported to be conducting, and both compounds show interesting collective effects. LiV_2O_4 is the only oxide heavy fermion system and LiTi_2O_4 is a superconductor [2–5].

For 4d and 5d transition metal oxides (TMOs), because the 4d/5d orbitals are spatially more extended, the on-site Coulomb repulsion energy U is smaller compared to the 3d oxide counterparts. A unique characteristic of 5d TMOs is that the energy scale of the spin-orbit coupling (SOC) is comparable to U , suggesting an interesting interplay among SOC, U ,

and electron bandwidth. Conventional intuition suggests that a 5d oxide is more metallic compared to its 3d counterpart due to the greater spatial extent of the 5d orbitals (therefore larger 5d bandwidth) and reduced Coulomb interaction. Many iridates, however, are magnetic insulators, a fact that has been attributed in part to the large SOC of iridium coupled with the $5d^5$ configuration of Ir^{4+} ions. In this case, the iridate electronic structure has been characterized using a j_{eff} description (SOC dominates and t_{2g} states split into half-filled $j_{\text{eff}} = 1/2$ and filled $j_{\text{eff}} = 3/2$ states) [6].

Relatively few undoped iridates possess a metallic state, suggesting that the localizing effect of SOC generally dominates the expected larger bandwidth. The iridium spinel compound CuIr_2S_4 is one example [7,8] and has been extensively investigated as a candidate for the quantum compass model [9] due in part to the mixed $\text{Ir}^{3+/4+}$ site arrangement. The perovskite SrIrO_3 is another example as a narrow-band semimetal [10]. Iridate oxide compounds that are normally insulating have been shown to become metallic by doping. For example, while BaIrO_3 is insulating, rare-earth R^{3+} ($R = \text{Gd}, \text{Eu}$) substitution for Ba^{2+} can induce a metallic state [11]. Another example is Rh doping in $\text{Sr}_2\text{Ir}_{1-x}\text{Rh}_x\text{O}_4$. Sr_2IrO_4 is an antiferromagnetic $j_{\text{eff}} = 1/2$ Mott insulator [12,13], however, Rh doping induces a metal-insulator transition due to hole doping in the Ir 5d $j_{\text{eff}} = 1/2$ band [14,15]. Sr_2IrO_4 has also been synthesized with oxygen vacancies, inducing an insulator-to-metal transition [16]. Clearly, the mixed valency of iridium in such examples plays a role in altering the interplay between bandwidth, SOC, and on-site Coulomb repulsion and driving a metal-insulator transition (MIT). So far, we have discussed local energetic attributes controlling

*Mas.subramanian@oregonstate.edu

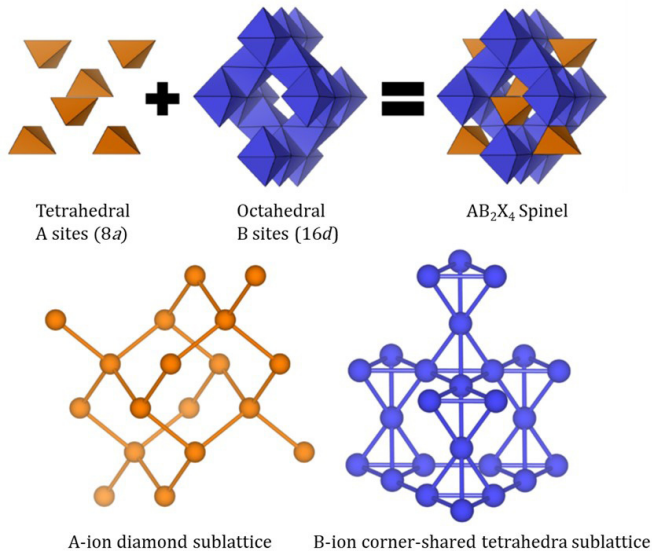


FIG. 1. Illustration of the AB_2X_4 spinel structure: isolated A-cation tetrahedral sites and the B_2X_4 rocksalt network where 1/2 of the octahedral sites are occupied (top). The A ions form a diamond sublattice and the B ions form a sublattice of corner-shared tetrahedra within the spinel structure (bottom).

the MIT, but the geometry of the lattice can also be important for charge itineracy. Just as geometrical frustration associated with nonbipartite lattices leads to ground state degeneracy in local moment systems, the analogous effect for conduction electrons is to create a flat band [17]. Therefore, the exploration of new frustrated structures that possess large SOC mixed valence ions is imperative.

In the present work we report on the synthesis, structure, and properties of the iridate-containing mixed B-site spinel oxide: $Cu[Ir_{1.498(2)}Cu_{0.502(2)}]O_4$. The results presented show a mixed $Cu^{1+/2+}$ and $Ir^{3+/4+}$ charge portioned picture with random Cu-Ir site disorder within the B_2O_4 rocksalt substructure. The magnetic properties reveal a strongly frustrated magnet at temperatures above the spin-glass-like behavior ($T_g = 49$ K). Electronic measurements and DFT theory reveal that a metallic/band description with reduced on-site Coulomb interactions should be used to describe the electronic ground state.

II. EXPERIMENT

Polycrystalline $Cu[Ir_{1.498(2)}Cu_{0.502(2)}]O_4$ was prepared via the synthesis of the hyperkagome structure $Na_4Ir_3O_8$ and then an ion-flux exchange approach using CuCl. The compounds Na_2CO_3 and IrO_2 with the correct stoichiometric ratio ($Na_4Ir_3O_8$) were ground and pressed into 10-mm-diameter pellets. The resulting pellet was fired at 750 °C for 16 h, ground, and then reheated to 1000 °C for 18 h before being quenched using a water bath. The resulting hyperkagome $Na_4Ir_3O_8$ sample was mixed with molar excess of CuCl and then fired at 450 °C under an argon flow. The sample was then washed with a dilute nitric acid solution to remove remaining NaCl and excess CuCl and Cu metal.

Phase analysis of powder samples was performed by x-ray diffraction using a Rigaku MiniFlex II diffractometer

with Cu $K\alpha$ radiation and a graphite monochromator for the diffracted beam. Synchrotron x-ray diffraction (Advanced Photon Source 11-BM-B) was collected at room temperature ($\lambda = 0.41283$ Å, $2\theta < 50^\circ$). Resistivity and Seebeck coefficient were measured from 300 to 600 K using an ULVAC ZEM-3 under a helium atmosphere. The resistivity below 300 K was measured using the four-wire technique and the internal resistance bridge in a Quantum Design PPMS. The electrical contacts were made using Ag epoxy. The susceptibility was defined as M/H where M is the dc magnetization, which was measured in a Quantum Design MPMS3 superconducting quantum interference (SQUID) magnetometer.

X-ray absorption spectra (XAS) at Cu- K and Ir- $L_{2,3}$ absorption edges were collected at room temperature in transmission geometry at the Advanced Photon Source of Argonne National Laboratory. Near-edge XAS data were collected at beamline 4-ID-D while extended x-ray absorption fine structure (EXAFS) spectra were collected at beamline 9-BM. For these measurements, fine powder samples were dispersed on multiple layers of tape then combined to achieve the desired effective sample thickness. At 4-ID-D, toroidal and flat Pd mirrors in combination with detuning of the second Si(111) crystal in the double crystal monochromator (DCM) were used to focus the x-ray beam to $100 \times 200 \mu m^2$ and reject high-energy harmonic radiation. At 9-BM, a Rh-coated toroidal mirror was used to focus the beam to $\sim 500 \times 500 \mu m^2$ and, in combination with detuning of the second crystal of the Si(111) DCM, reject high-energy harmonic radiation. At both 4-ID-D and 9-BM, ionization chambers were used as detectors. The energy resolution of a Si(111) monochromator at these absorption edges is in the 1.2–1.5-eV range, but the repeatability in energy scans is better than 0.1 eV. Reference samples of IrO_2 (Ir 4+ valence), Ba_2YIrO_6 (Ir 5+ valence), CuO (Cu 2+ valence), and Cu_2O (1+ valence) were used to assess the unknown charge state of Ir and Cu ions in the spinel sample. XAS data at Cu- $L_{2,3}$ edges were collected at room temperature at beamline 29-ID of the Advanced Photon Source at Argonne National laboratory using partial fluorescence yield (PFY) with a multichannel plate detector placed in the horizontal plane at 90° with the incoming, horizontally polarized x-ray beam. Measurements were carried out on powder samples mounted on carbon tape, as well as on samples embedded in indium foil, yielding consistent data.

The resonant inelastic x-ray scattering (RIXS) measurements were performed using the RIXS spectrometer at the 27-ID beamline of the Advanced Photon Source where the sample, analyzer, and detector are positioned in the Rowland geometry [18,19]. The diamond (111) high-heat-load monochromator reflects x rays from two in-line undulators into a high-resolution monochromator. The two-bounce monochromator of single monolithic Si(844) channel-cut crystal produces an energy bandpass of 14.8 meV at 11.215 keV. The beam is then focused by a set of Kirkpatrick-Baez mirrors, yielding a typical spot size of $10 \times 40 \mu m^2 (v \times h)$ at the sample. A horizontal scattering geometry is used with the incident photon polarization in the scattering plane. All data were collected with the 90° scattering angle to minimize the contribution from the Thompson elastic scattering. The Si(844) diced spherical analyzer and

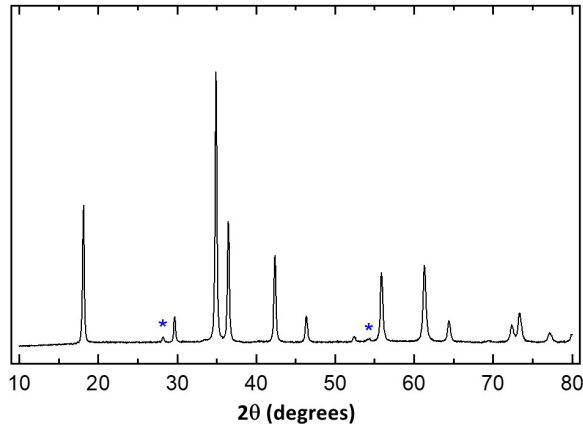


FIG. 2. Powder XRD pattern of $\text{Cu}[\text{Ir}_{1.498(2)}\text{Cu}_{0.502(2)}]\text{O}_4$ sample. Blue asterisk symbol indicates a small presence of IrO_2 impurity phase.

the position-sensitive silicon microstrip detector produce an overall energy resolution of full width at half maximum = 30 meV.

Density functional theory (DFT) calculations were performed using Vienna *Ab-initio* Simulation Package (VASP) [20,21]. The Perdew-Burke-Ernzerhof (PBE) implementation [22] was used as the exchange-correlation functional. To include the strong Coulomb interaction effect of d orbitals, we used the Hubbard U values of 5 eV for the Cu $3d$ orbital and 2.5 eV for the Ir $5d$ orbital. We also used the Hund's coupling J values of 0.8 eV for the Cu $3d$ orbital and 0.4 eV for the Ir $5d$ orbital. To simulate the site-disorder effect of Cu and Ir ions within the octahedral sites, we build the supercell of the spinel structure containing 12 Cu, 12 Ir, and 32 O ions. The Cu and Ir ions are randomly distributed with the ratio of 1:3 among the octahedral sites. The density of states is computed for each random structure and averaged for the comparison to the experimental spectra. The gamma-centered Monkhorst-Pack k -point mesh of $6 \times 6 \times 6$ was adopted for each supercell structure. The energy-cutoff for the plane-wave basis was used as 400 eV.

III. RESULTS

A. Structural analysis

Powder x-ray diffraction pattern of $\text{Cu}[\text{Ir}_{1.498(2)}\text{Cu}_{0.502(2)}]\text{O}_4$ reveals face-centered-cubic structure with space group $Fd\bar{3}m$ (Fig. 2). The trace IrO_2 impurity phase was detected in the diffraction pattern upon magnification (Fig. 2, asterisk symbol). To determine the crystal structure, Rietveld refinements were performed on synchrotron XRD data collected at APS beamline 11-BM-B using the GSAS program [23,24]. Room temperature synchrotron XRD was collected up to 50° in 2θ . A pseudo-Voigt peak shape profile was chosen, and parameters refined to obtain the best fit to the collected data. The space group was refined to be $Fd\bar{3}m$ with cubic lattice dimensions of 8.5762(1) Å. The resulting synchrotron XRD Rietveld refinement for $\text{Cu}[\text{Ir}_{1.498(2)}\text{Cu}_{0.502(2)}]\text{O}_4$ is shown in Fig. 3. For the refined fit, the R_{wp} factor was 5.65% and the goodness of fit χ^2

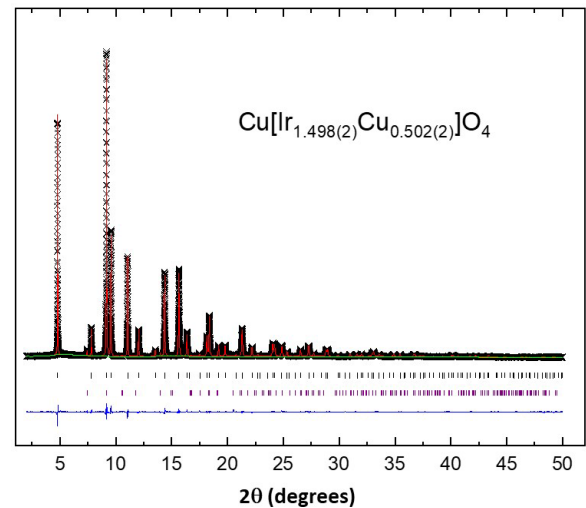


FIG. 3. Synchrotron Rietveld refinement of $\text{Cu}[\text{Ir}_{1.498(2)}\text{Cu}_{0.502(2)}]\text{O}_4$ sample at room temperature ($\lambda = 0.41283$ Å). Observed (black crosses) and calculated (solid red line) profiles, background (green), and difference curve ($I_{\text{obs}} - I_{\text{calc}}$) (blue) are shown. The vertical bars indicate the expected reflection positions for spinel ($Fd\bar{3}m$) phase (black) and IrO_2 impurity phase (purple).

was 1.4, confirming that the $Fd\bar{3}m$ structure model suitably fits the compound. The detailed results are given in Table I. Refined structure parameters are in accordance with other analogous cubic $Fd\bar{3}m$ spinel oxide structures [25–27].

From the refined parameters provided in Table I, the tetrahedral $8a$ site was refined to be fully occupied by copper. Iridium is too large for a tetrahedral site and any addition

TABLE I. Rietveld refinement results of synchrotron XRD diffraction data for $\text{Cu}[\text{Ir}_{1.498(1)}\text{Cu}_{0.502(1)}]\text{O}_4$.^{a,b}

Composition	$\text{Cu}[\text{Ir}_{1.498(1)}\text{Cu}_{0.502(1)}]\text{O}_4$
Space group	$Fd\bar{3}m$
$R_{\text{wp}}(\%)/\chi^2$	5.65/1.41
$a = b = c(\text{Å})$	8.5762(1)
$V(\text{Å}^3)$	630.79(1)
O, x	0.26068(9)
Cu ($8a$) occ.	1
Ir ($16d$) occ.	0.7490(2)
Cu ($16d$) occ.	0.2510(2)
Cu ($8a$) $U_{\text{iso}}(\text{Å}^2)$	0.01636 (2)
Cu/Ir ($16d$) $U_{\text{iso}}(\text{Å}^2)$	0.009581(3)
O $U_{\text{iso}}(\text{Å}^2)$	0.02051(2)
Cu/Ir($16d$)-O (Å)	2.0565(7)
Cu($8a$)-O (Å)	2.0155(1)
O-Cu($8a$)-O ($^\circ$)	109.47(1)
O-Cu($16d$)-O ($^\circ$)	95.22(4)
O-Ir-O ($^\circ$)	84.78(4)

^aSynchrotron XRD diffraction data collected at APS 11-BM-B (room temperature).

^bFor $Fd\bar{3}m$, AM_2O_4 crystal structure refined in space group with $A(\text{Cu})$ at $8a$ (1/8,1/8,1/8), $M(\text{Cu}/\text{Ir})$ at $16d$ (1/2,1/2,1/2), and O at $32e$ (x, x, x) sites.

of iridium in the $8a$ site proved not stable in the refinement. Incorporation of copper on the octahedral $16d$ site did result in an overall more stable refinement. The resulting $16d$ refined occupancies reveal a mixed Cu-Ir site disorder within the B_2O_4 rocksalt substructure: 75% of the respective site is occupied by iridium with the remaining 25% occupied by copper.

Semiquantitative fits of EXAFS data were carried out using theoretical standards in order to provide validation of the site occupancies found in the XRD refinements. Theoretical Cu- K - and Ir- L_3 -edge EXAFS scattering amplitudes and phases were generated with the FEFF6 code [28] using an 8-Å radius atomic cluster based on the space group, lattice parameters, and atomic positions obtained from XRD refinements (Table I). The atomic cluster included both Ir and Cu atoms in the $16d$ octahedral sites with a 3:1 ratio. In the fits, the $8a$ tetrahedral sites are fully occupied by Cu atoms, whereas the relative Ir/Cu occupation of $16d$ octahedral sites was an adjustable parameter. Other adjustable parameters were Debye-Waller factors and an overall isotropic lattice expansion/contraction. Cu (Ir) EXAFS data and theoretical standards in the k range 2–14 (2–16) Å⁻¹ were weighted by k^2 and Fourier transformed for fitting in real space using the rather constrained model described above. Figure 4 shows data and models in real space (real and imaginary parts, as well as magnitude, of the complex Fourier transforms) as well as back Fourier transformed data and model utilizing real space data in the 1–5-Å region. The fitted occupation of Cu (Ir) atoms in $16d$ octahedral sites is 0.27 ± 0.05 (0.73 ± 0.14) in good agreement with XRD results. The isotropic model for interatomic distances yields a small contraction of the lattice of order 1%. Fitted Debye-Waller factors are in the 0.003–0.015-Å² range. The semiquantitative EXAFS modeling provides a reasonable description of both Cu- K - and Ir- L_3 -edge EXAFS spectra and is consistent with the site occupancies found in Rietveld refinements.

B. Electronic properties

Temperature dependent resistivity and Seebeck measurements are shown in Fig. 5. Resulting electrical properties reveal a metallic state within the 50–550-K range with a Kondo-like effect below $T = 50$ K.

X-ray absorption spectroscopy (XAS) measurements at the Cu $L_{2,3}$, Cu K , and Ir $L_{2,3}$ absorption edges were used to provide an estimate of copper and iridium valence. Figure 6 shows Cu- $L_{2,3}$ -edge x-ray absorption data for Cu[_{1.498(2)}Ir_{0.502(2)}]O₄ spinel system, together with Cu 1+ and Cu 2+ reference spectra taken from Ref. [29]. Data were normalized to Cromer-Lieberman calculations of the single-atom absorption cross section [30] and clearly show copper in mostly a 2+ state. The fraction of Cu 2+ and Cu 1+ ions was estimated to be 75(10)%: 25(10)% from white line intensity ratios in sample and references, averaged over $L_{2,3}$ edges.

The Cu- K -edge x-ray absorption data (Fig. 7) also shows copper predominately in a 2+ state. As shown in the right inset of Fig. 7, Cu₂O has a strong pre-edge peak. This pre-edge peak is not observed in CuO, and there is a small peak in the derivative for the Cu[_{1.498(2)}Ir_{0.502(2)}]O₄ spinel system. In addition, the main edge position (Fig. 7, derivative plot inset),

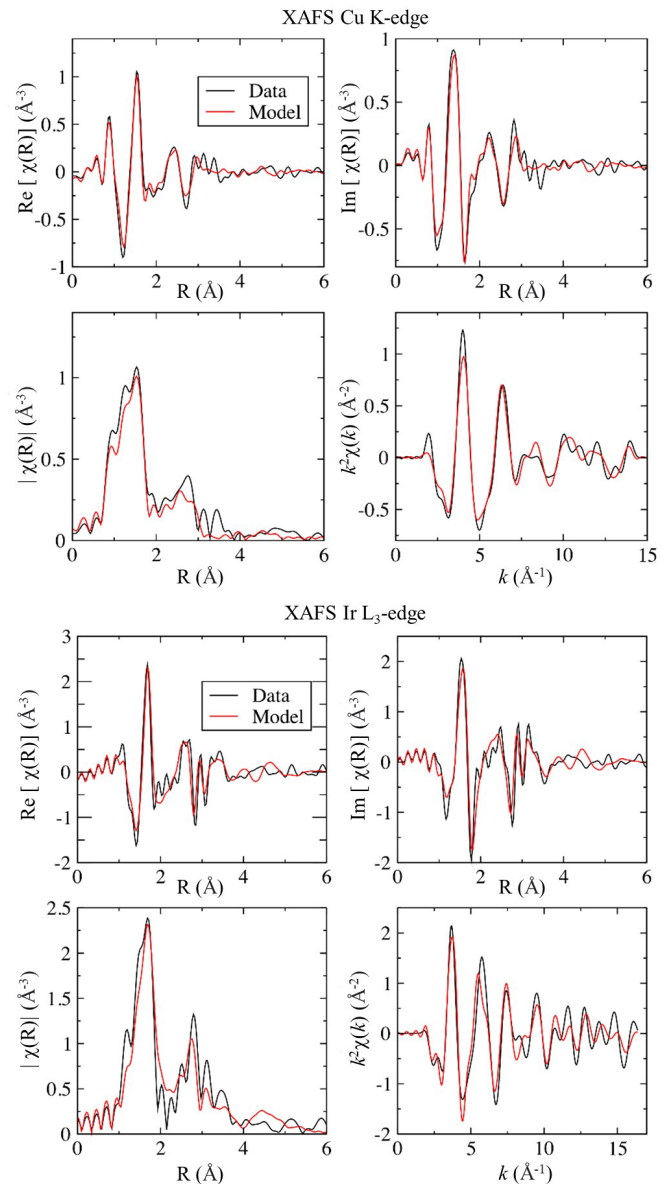


FIG. 4. Cu- K -edge and Ir- L_3 -edge EXAFS data and model. Real and imaginary parts, as well as magnitude, of the (complex) Fourier transform of k^2 weighted EXAFS data and model are shown in the real space plots, and back Fourier transformed data and model are shown in photoelectron wave number (k) space. Black line: data; red line: constrained model using the Ir/Cu partitioning and distances obtained in refinements of XRD data.

further suggests Cu in a predominant 2+ state. A weighted average of Cu 1+ and Cu 2+ reference spectra is shown in Fig. 7 to illustrate the enhancement of the pre-edge peak with increasing Cu 1+ content. As shown, if the Cu 1+ content is significantly larger than 10%, a sharp pre-edge signature would exist in the data. Such a sharp pre-edge signature does not exist for Cu[_{1.498(2)}Ir_{0.502(2)}]O₄, thus indicating a minority Cu 1+ component, consistent with Cu- L -edge data. While the Cu 2+ component clearly dominates, a more accurate determination of the 1+ to 2+ ratio is difficult from these measurements, not only due to the different character of sample and references (hybridized metallic versus ionic

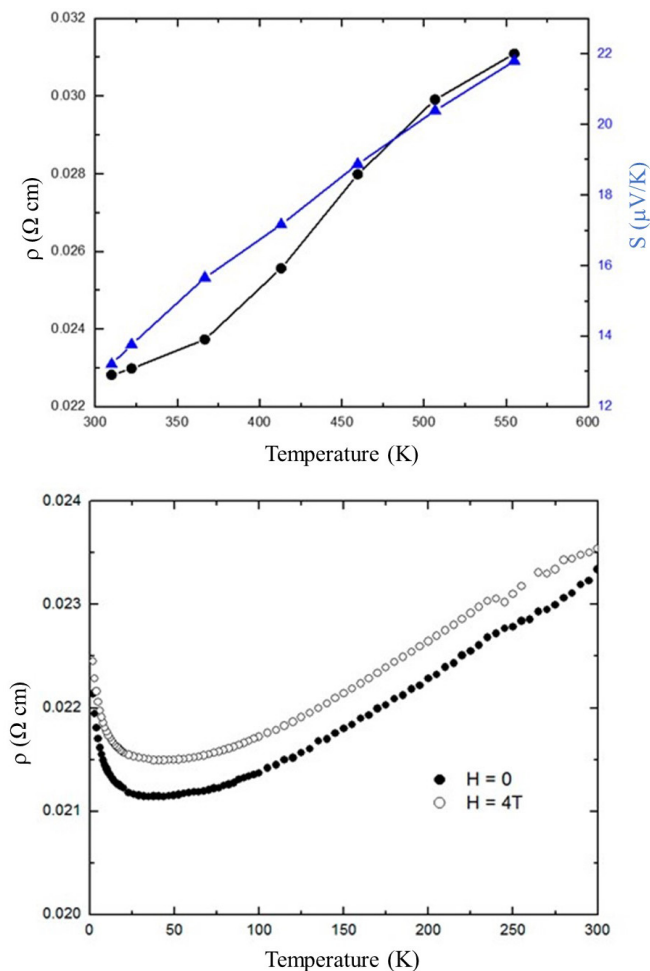


FIG. 5. Top: High temperature resistivity (black circles) and Seebeck (blue triangles) data of $\text{Cu}[\text{Ir}_{1.498(2)}\text{Cu}_{0.502(2)}]\text{O}_4$ sample from ~ 300 to ~ 550 K. Bottom: Resistivity vs temperature for $\text{Cu}[\text{Ir}_{1.498(2)}\text{Cu}_{0.502(2)}]\text{O}_4$ in the range 2–300 K under 0- and 4-T field.

insulators), but also due to possible distortions to Cu-L-edge data from self-absorption effects (see Discussion section).

XAS measurements at the Ir- $L_{2,3}$ absorption edges ($2p_{1/2,3/2} \rightarrow 5d$ resonant excitation) were used to provide an estimate of Ir valence. As shown in Fig. 8, the Ir- $L_{2,3}$ edge x-ray absorption spectra for $\text{Cu}[\text{Ir}_{1.498(2)}\text{Cu}_{0.502(2)}]\text{O}_4$ together with Ir 4+ and Ir 5+ reference spectra clearly show iridium in an oxidation state less than 4+. By analyzing energy shifts in XAS peak position and XAS peak derivative at both L_3 and L_2 edges in the spinel sample and reference compounds we estimate Ir oxidation state of $+3.6 \pm 0.2$.

The integral of white line intensities over Ir- $L_{2,3}$ edges is proportional to the number of $5d$ holes. For a polycrystalline sample, where relative orientation of crystalline axes and x-ray linear polarization is angular averaged, the isotropic sum rule (regardless of crystal symmetry) is given by $I_{L_3} + I_{L_2} = CN$ where $I_{L_{2,3}}$ are integrated intensity of $L_{2,3}$ white lines, N is the number of $5d$ holes, and C is the square of the radial part of the $2p \rightarrow 5d$ matrix element [31]. We calculated the integrated intensity under $L_{2,3}$ white lines in the spinel sample and reference compounds by fitting the XAS data using a combination of broadened step function to simulate the single

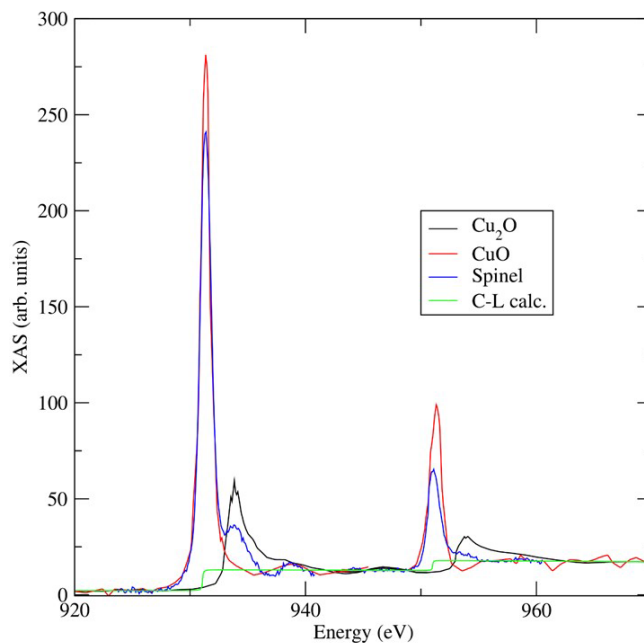


FIG. 6. Cu- $L_{2,3}$ -edge x-ray absorption data for $\text{Cu}[\text{Ir}_{1.498(1)}\text{Cu}_{0.502(1)}]\text{O}_4$ spinel system measured in partial fluorescence yield (PFY) together with Cu 1+ and Cu 2+ reference spectra taken from the literature (Ref. [29]). Data were normalized to Cromer-Liberman (C-L) calculations of the single-atom x-ray absorption cross section (Ref. [30]).

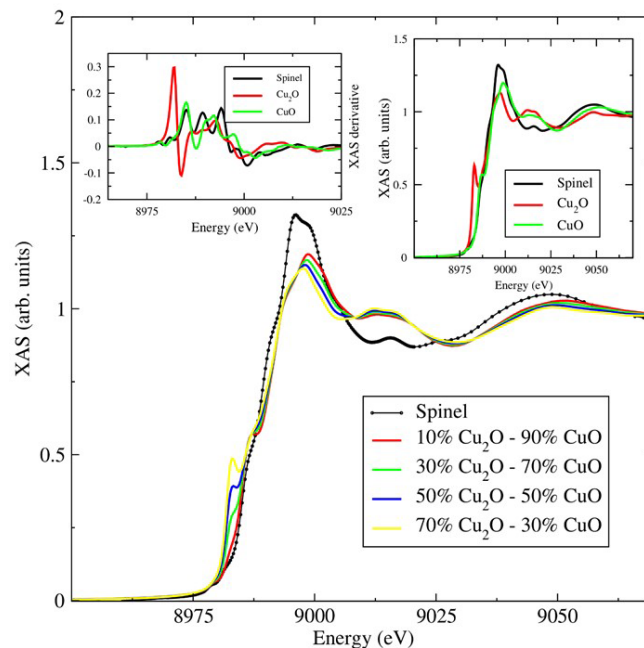


FIG. 7. Cu- K -edge x-ray absorption spectra for $\text{Cu}[\text{Ir}_{1.498(1)}\text{Cu}_{0.502(1)}]\text{O}_4$ spinel system together with Cu 1+ and Cu 2+ reference spectra (right inset). The derivatives of these spectra are shown in the left inset. The main panel shows weighted averages of Cu +1 and +2 reference data to illustrate the expected enhancement of the pre-edge peak with increasing Cu 1+ content.

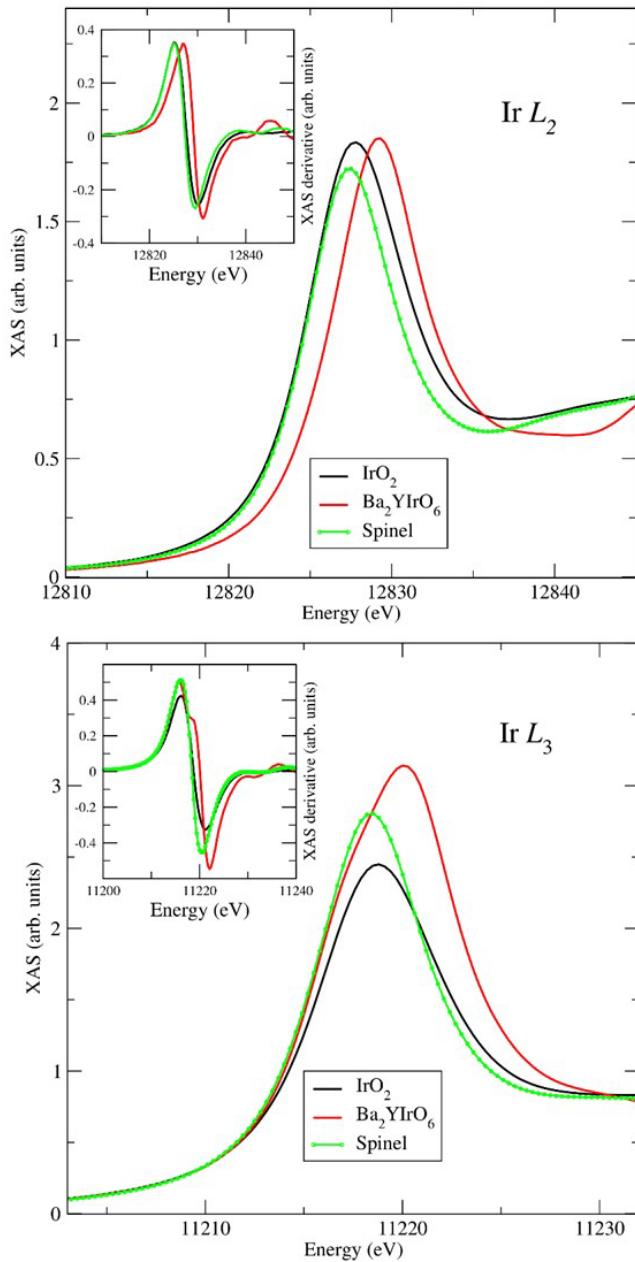


FIG. 8. XAS measurements at the Ir- $L_{2,3}$ absorption edges on $\text{Cu}[\text{Ir}_{1.498(2)}\text{Cu}_{0.502(2)}]\text{O}_4$ and two reference compounds with known oxidation state. The insets show the first derivatives of the XAS data.

ion absorption jump, and Gaussian function to simulate the resonant, white line, fine structure. The ratio of the integrals in the spinel compound to that in the reference compounds with known hole counts can be used to estimate the number of holes. This results in $5d$ hole values in the 3.8–4.5 range, depending on whether the $5+$ or $4+$ reference sample is used. The corresponding valence is in the 3–3.5+ range. Although imprecise, the hole count estimate is consistent with a valence significantly below $4+$, and is in reasonable agreement with the estimates from XAS peak shifts.

Finally, the ratio of L_3 to L_2 white line intensity, also known as the isotropic branching ratio (BR), provides a measure of the relevance of SOC interactions in the $5d$ band [32]. If SOC

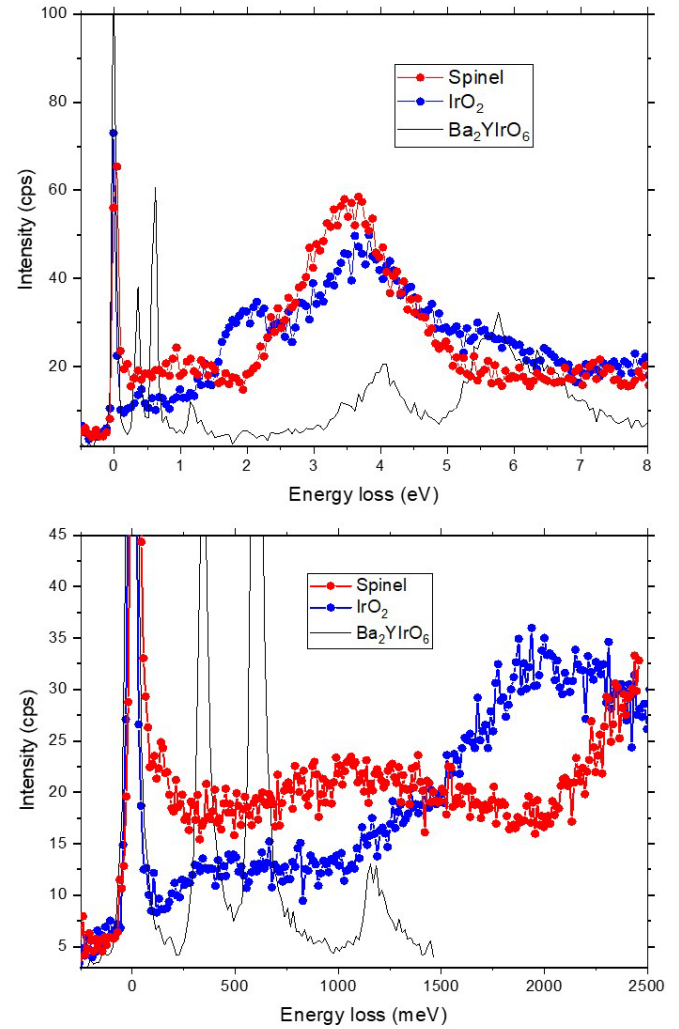


FIG. 9. RIXS wide (top) and narrow (bottom) ranges of the energy loss spectra for the $\text{Cu}[\text{Ir}_{1.498(2)}\text{Cu}_{0.502(2)}]\text{O}_4$ spinel and IrO_2 and Ba_2YIrO_6 systems.

interactions are negligible, the isotropic branching ratio equals 2. Theoretically, the reduction in BR for Ir ions in octahedral crystal field in going from $5+$ to $3+$ charge state is expected to be a factor of ~ 1.6 [32,33]. The BR value for Ba_2YIrO_6 , where Ir is in a $5+$ state, is 3.8 while that of the spinel sample is 2.4(1), a ratio of 1.6 indicating an Ir charge state close to $3+$ assuming an ionic picture. While it is difficult to assign a precise Ir valence due to the spread in values from different approaches (XAS peak shift, hole count, branching ratio), it is quite clear that the Ir valence is significantly lower than $4+$.

Resonant inelastic x-ray scattering (RIXS) was used to investigate the electronic structure of the spinel system. Figure 9 shows the collected RIXS data for $\text{Cu}[\text{Ir}_{1.498(2)}\text{Cu}_{0.502(2)}]\text{O}_4$ spinel system, together with IrO_2 and Ba_2YIrO_6 reference spectra [34–36]. In all spectra, broad peak features above 3 eV are interpreted as originating from the excitation between Ir $5d$ orbital states split by the octahedral crystal field and charge-transfer excitation [35–39]. For the low energy region, the Ba_2YIrO_6 spectrum shows well-defined, sharp, and discrete excitations of the t_{2g} multiplet levels in the d^4 configuration where the effects of the

local interactions (SOC, Hund's coupling, and U) dominate the orbital overlap, leading to a SOC Mott insulating ground state [34,35]. On the other hand, for the spinel system and IrO_2 , the low energy region is characterized by broad peak features. Not visible are sharp excitation peaks related to the SOC split states (so-called j_{eff} states) which are observed in insulating iridium oxides [34,35,39,40]. According to the density functional theory calculations of IrO_2 [41], the bandwidth of the t_{2g} state is as large as 10 eV and dominates the effects of the local interactions, giving rise to a metallic ground state and the broad low energy feature of the IrO_2 RIXS spectrum. Likewise, the broad low energy feature of the spinel spectrum is interpreted to reflect the strong orbital overlap and reduced on-site Coulomb interactions within Ir/Cu d states, giving rise to a metallic ground state in the spinel system. The spinel system spectrum shows a low energy shoulder below 300 meV which is not visible in the IrO_2 and Ba_2YIrO_6 spectra. This low energy shoulder feature of the spinel system is in close resemblance to that of metallic pyrochlore iridates such as $\text{Eu}_2\text{Ir}_2\text{O}_7$ and $\text{Pr}_2\text{Ir}_2\text{O}_7$ at room temperature [42,43]. The shoulder feature of metallic pyrochlore iridates is interpreted as incoherent magnetic excitations of short-lived paramagnetic fluctuations. The observed low energy shoulder feature of the spinel system is suggested to originate from short-range magnetic interactions of the geometrically frustrated spinel system. In addition, the low energy shoulder feature at room temperature suggests that short-range magnetic correlations of the spinel system survive into the paramagnetic state with specific short-range dynamics which is plausibly related to the observed spin-glass-like behavior.

C. Magnetic properties

The magnetic susceptibility is shown in Fig. 10. As can be seen in Fig. 10(a), spin-glass-like freezing is seen at $T_g = 49$ K, as evidenced by hysteresis between zero-field-cooled and field-cooled data. The behavior for $T > T_g$ resembles that of a strongly frustrated magnet. Since the compound possesses a mixture of Cu^{1+} , Cu^{2+} , Ir^{3+} , and Ir^{4+} ions, and since Cu^{1+} and Ir^{3+} are nonmagnetic, one need only consider Cu^{2+} and Ir^{4+} in the effective moment approximation for $\text{Cu}_{0.375}^{1+}\text{Cu}_{1.125}^{2+}\text{Ir}_{0.6}^{3+}\text{Ir}_{0.9}^{4+}\text{O}_4$, where the contributions to the stoichiometry for each ion type [75(10)%: 25(10)% for Cu 2+/Cu 1+ ions] is provided by the above XAS data. Thus, we assume that these two species contribute to $\chi(T)$ as

$$1.125p_{\text{Cu}^{2+}}^2 + 0.9p_{\text{Ir}^{4+}}^2 = \frac{3k_B}{\mu_B^2 N_A} (d\chi^{-1}/dT)^{-1},$$

where $p_{\text{Cu}^{2+}}$ and $p_{\text{Ir}^{4+}}$ are the effective moments for Cu^{2+} and Ir^{4+} respectively, k_B is Boltzmann's constant, μ_B is the Bohr magneton, and N_A is Avogadro's number. For this calculation we use the slope of $\chi^{-1}(T)$ in the range $125 \text{ K} < T < 250 \text{ K}$ shown by the fit line in Fig. 10(b). The effective moments for Cu^{2+} and Ir^{4+} are each $\sqrt{3}\mu_B$, and we find that this equation is only satisfied by subtracting a constant of 3.65×10^{-4} emu/mole from $\chi(T)$. In the present case, such a constant can only arise from a Pauli-like susceptibility, the magnitude of which implies a Sommerfeld specific heat coefficient of $\gamma = 27 \text{ mJ/mole K}^2$. This is substantially larger than that of

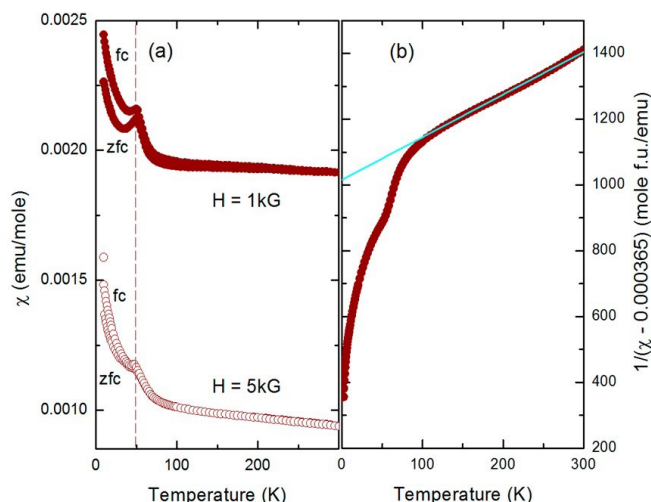


FIG. 10. (a) The zero-field-cooled (zfc) and field-cooled (fc) susceptibility vs temperature for $\text{Cu}[\text{Ir}_{1.498(2)}\text{Cu}_{0.502(2)}]\text{O}_4$ as measured at two different magnitudes of applied field. The hysteresis below the peak at 49 K is evidence for spin glass freezing. (b) The inverse susceptibility with a constant 3.65×10^{-4} subtracted from $\chi(T)$ vs temperature. The straight line is a least squares fit as discussed in the text.

weakly correlated metals for which $\gamma \approx 1 \text{ mJ/mole K}^2$, but is in the range of other $4d$ and $5d$ conducting oxides [44].

D. Electronic structure from density functional theory

In an effort to reconcile the valence state analysis with the electronic measurements, we have applied density functional theory (DFT) to our study of the $\text{Cu}[\text{Ir}_{1.498(2)}\text{Cu}_{0.502(2)}]\text{O}_4$ spinel system. From our DFT + U + SO result (Fig. 11), the electron occupation of Cu tetrahedral sites (Cu1) is 9.77 (0.23 holes), corresponding to an effective Cu valence of 1.23+. The electron occupation of the Cu octahedral sites (Cu2) is 9.31 (0.69 holes), corresponding to an effective Cu valence of 1.69+. For iridium, the $5d$ electron occupation in t_{2g} states is 5.55 (0.45 holes) providing an effective valence for Iridium of 3.45+. Without the SO effect, the electron occupation of the Cu1 $3d$ orbital is slightly decreased (~ 0.06) while the Ir $5d$ orbital occupation is slightly increased (~ 0.07). The DFT results show sizable hybridization between Cu $3d$ and Ir $5d$ states.

IV. DISCUSSION

The atomic, structural, and electronic (transport, magnetometry, DFT) results provide a comprehensive and congruous description on the properties of the synthesized iridium spinel oxide system. Overall, the XAS measurements agree well with the refined $Fd\bar{3}m$ structure and site occupancies. From Cu- $L_{2,3}$ - and Cu- K -edge spectroscopy, the fraction of Cu^{2+} and Cu^{1+} ions can be reasonably estimated to be 75(10)%: 25(10)%, or an average Cu valence of $+1.7 \pm 0.2$. Assuming 75(10)% of Cu is in a 2+ state (with the remaining in a 1+ state), the composition $\text{Cu}[\text{Ir}_{1.498(2)}\text{Cu}_{0.502(2)}]\text{O}_4$ refined from XRD data would suggest an average iridium oxidation state of $+3.6 \pm 0.2$, which is consistent with the findings from

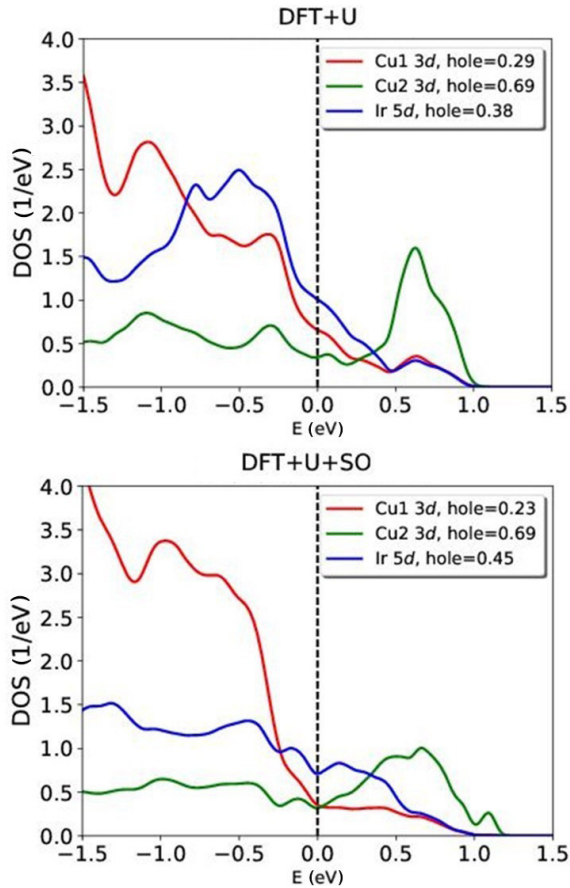


FIG. 11. Density of states obtained using DFT + U (top) and DFT + U + SO (bottom) calculations on $\text{Cu}[\text{Ir}_{1.498(2)}\text{Cu}_{0.502(2)}]\text{O}_4$ spinel system. Cu1 means the Cu ion in the tetrahedral site and Cu2 means the Cu ion in the octahedral site. Hole occupancies in d orbitals are obtained by integrating the partial DOS above the Fermi level.

Ir- L -edge XAS data. Additionally, the constrained EXAFS models based on site occupancies found in the Rietveld refinement provide a decent description of the Cu- K - and Ir- L_3 -edge EXAFS spectra. As mentioned earlier, Cu valence estimates from PFY L -edge data can be affected by self-absorption. Similarly, Cu valence estimates from Cu- K -edge data may be affected by different character (metallic vs insulating) of spinel and reference samples. We therefore deem the Cu valence estimates to be less accurate than the Ir valence estimates.

The RIXS spectra clearly confirm the metallic nature of the spinel. From the RIXS work, it can be concluded that a description in terms of j_{eff} states is not a good basis for the electronic ground state; rather a metallic/band description with reduced on-site Coulomb interactions should be used. Additionally, the RIXS spectra point to spin-glass-like behavior, established in the magnetic susceptibility data.

A magnetic moment of $2.53\mu_B$ determined from the susceptibility measurement is consistent with g factors of $\sqrt{3}$ for each Cu^{2+} and Ir^{4+} . If the Pauli-like constant of 3.65×10^{-4} is not subtracted from the susceptibility, the moment is $3.61\mu_B$, which implies even larger individual moments for the two magnetic ions. If smaller moments than $\sqrt{3}$ are used, then

a different value for the Pauli-like constant will need to be subtracted in order to yield effective moment behavior. Since it is uncertain at this time as to the precise low moment to use, it is considered most practical to perform a conventional analysis. It is not too surprising, however, to see large values for the effective moments, even though the orbitals are delocalized since this is one of the features of heavy-fermion systems [2,4]. Such systems appear local-moment-like at high T even though they are strongly hybridized and itinerant.

The establishment of two different set of spins—interpreted from resistivity and susceptibility measurements—is considered reasonable as resistivity is most sensitive to zone-boundary, $q \sim \pi$, excitations, whereas the susceptibility is a $q = 0$ probe. As the spin-glass phase implies the existence of impurity spins, it is not unreasonable to consider that some spins decouple from the spin-glass phase and instead develop a Kondo coupling to the itinerant electrons. Since our interpretation is in terms two different set of spins, the Kondo effect is clearly dominated by freezing of the local moments, as might be expected since the Kondo signature is that of a magnetic singlet.

The DFT results agree with the electronic results. The Ir valence calculated from the DFT work match the Ir valence determined from XAS measurements. Assuming a 2:1 ratio for Cu occupancy at tetrahedral and octahedral sites, the DFT results imply an average Cu valence of +1.38. Thus, the DFT results for the Cu valence are lower but comparable to the Cu valence estimated from the XAS measurements. However, as stated previously, the Cu valence estimated from XAS is somewhat less reliable. Regardless, the DFT results show sizable hybridization between Cu 3d and Ir 5d states, consistent with the metallic nature of the spinel.

Both $\text{Cu}^{1+/2+}/\text{Ir}^{3+/4+}$ charge partitioning and Cu-Ir site disorder within the geometrically frustrated B_2O_4 rocksalt substructure play an important role in the electronic behavior of this spinel system. If, say, a description in terms of j_{eff} states was a good basis for the electronic ground state, Cu would oxidize from 1+ to 2+ and dope electrons into the upper Hubbard band of Ir $j_{\text{eff}} = 1/2$ states because the Ir t_{2g} states are lower in energy than the Cu 3d states, therefore reducing electron correlations and enhancing conductivity. Similar arguments have been made for Ln-doped BaIrO_3 [11], Rh-doped Sr_2IrO_4 [14,15], and static compression work on the hyperkagome $\text{Na}_3\text{Ir}_3\text{O}_8$ [45]. However, this self-doping argument where the Ir 5d and Cu 3d hybridize predominately with oxygen p orbitals is a more simplified localized picture. The situation is clearly more complicated if the Ir 5d and Cu 3d hybridize themselves, which is strongly exhibited in the RIXS and DFT work presented. Regardless, the observed charge partitioned $\text{Ir}^{3+/4+}$ framework clearly influences the interplay between bandwidth, SOC, and on-site Coulomb repulsion effects, promoting strong orbital overlap and reduced on-site Coulomb interactions within Ir/Cu d states, resulting in a metallic ground state in the spinel system. Additionally, the geometrical frustration associated with the determined nonbipartite lattice promotes ground state degeneracy and supports the picture of a strongly frustrated magnet.

The present work clearly demonstrates how local energetic attributes and lattice geometry influence charge itineracy and the electronic behavior of the system. Geometrical frustration

in electronic degrees of freedom has been a major topic in the field of condensed matter physics, and the spinel structure has offered fascinating insights in terms of their unusual physical properties due in part to geometrical frustration. However, though many $3d/4d$ spinel structures have been extensively studied, to our knowledge, a $5d$ spinel oxide has never been reported. The significance of this work is further highlighted by the fact that only two other spinel oxides are known to be conducting [2–5] and relatively few iridates possess iridium in a $3+$ valence state [11–16]. In summary, the reported properties and DFT theory clearly confirm the metallic nature of this spinel and provide direct evidence of a metallic iridate spinel oxide compound and with Ir in a $3+/4+$ charge partitioned state. We hope this study will encourage the pursuit of other similar versions of this compound and the exploration of new frustrated $5d$ spinel oxide compounds.

V. CONCLUSION

We have presented an example of iridium on a mixed B-site spinel oxide lattice, $\text{Cu}[\text{Ir}_{1.498(2)}\text{Cu}_{0.502(2)}]\text{O}_4$, and have characterized it with atomic, structural, and electronic probes. The results presented show a mixed $\text{Cu}^{1+/2+}$ and $\text{Ir}^{3+/4+}$ charge partitioned picture with random Cu-Ir site disorder within the B_2O_4 rocksalt substructure. This compound is

metallic, and a frustrated system exists at temperatures above the spin-glass-like behavior. These results strongly show that the mixed iridium charge partitioned picture, along with Cu-Ir site disorder within the geometrically frustrated lattice, play an important role in the electronic behavior of this spinel system. This work highlights the importance for the exploration of new frustrated structures that possess large SOC mixed valence ions.

ACKNOWLEDGMENTS

The work performed at Oregon State University was supported by National Science Foundation Grant No. DMR-1508527. The work performed at University of California Santa Cruz was supported by U.S. Department of Energy Grant No. DE-SC0017862. The work performed at the Advanced Photon Source was supported by the U.S. Department of Energy, Office of Science, and Office of Basic Energy Sciences under Contract No. DE-AC02-06CH11357. DFT work was supported by the U.S. Department of Energy, Office of Science, Basic Energy Sciences, Materials Sciences and Engineering Division. We acknowledge the computing resources provided on Bebop, a high-performance computing cluster operated by the Laboratory Computing Resource Center at Argonne National Laboratory.

-
- [1] P. W. Anderson, Ordering and antiferromagnetism in ferrites, *Phys. Rev.* **102**, 1008 (1956).
- [2] C. Urano, M. Nohara, S. Kondo, F. Sakai, H. Takagi, T. Shiraki, and T. Okubo, LiV_2O_4 Spinel as a Heavy-Mass Fermi Liquid: Anomalous Transport and Role of Geometrical Frustration, *Phys. Rev. Lett.* **85**, 1052 (2000).
- [3] K. Jin, G. He, X. Zhang, S. Maruyama, S. Yasui, R. Suchoski, J. Shin, Y. Jiang, H. S. Yu, J. Yuan, L. Shan, F. V. Kusmartsev, R. L. Greene, and I. Takeuchi, Anomalous magnetoresistance in the spinel superconductor LiTi_2O_4 , *Nat. Commun.* **6**, 7183 (2015).
- [4] S. Kondo, D. C. Johnston, C. A. Swenson, F. Borsa, A. V. Mahajan, L. L. Miller, T. Gu, A. I. Goldman, M. B. Maple, D. A. Gajewski, E. J. Freeman, N. R. Dilley, R. P. Dickey, J. Merrin, K. Kojima, G. M. Luke, Y. J. Uemura, O. Chmaissem, and J. D. Jorgensen, LiV_2O_4 : A Heavy Fermion Transition Metal Oxide, *Phys. Rev. Lett.* **78**, 3729 (1997).
- [5] D. C. Johnston, H. Prakash, W. H. Zachariasen, and R. Viswanathan, High temperature superconductivity in the Li-Ti-O ternary system, *Mater. Res. Bull.* **8**, 777 (1973).
- [6] B. J. Kim, Hosub Jin, S. J. Moon, J.-Y. Kim, B.-G. Park, C. S. Leem, Jaeju Yu, T. W. Noh, C. Kim, S.-J. Oh, J.-H. Park, V. Durairaj, G. Cao, and E. Rotenberg, Novel $J_{\text{eff}} = 1/2$ Mott State Induced by Relativistic Spin-Orbit Coupling in Sr_2IrO_4 , *Phys. Rev. Lett.* **101**, 076402 (2008).
- [7] G. Jackeli and G. Khaliullin, Mott Insulators in the Strong Spin-Orbit Coupling Limit: From Heisenberg to a Quantum Compass and Kitaev Models, *Phys. Rev. Lett.* **102**, 017205 (2009).
- [8] P. G. Radaelli, Y. Horibe, M. J. Gutmann, H. Ishibashi, C. H. Chen, R. M. Ibberson, Y. Koyama, Y.-S. Hor, V. Kiryukhin, and S.-W. Cheong, Formation of isomorphous Ir^{3+} and Ir^{4+} octamers and spin dimerization in the spinel CuIr_2S_4 , *Nature (London)* **416**, 155 (2002).
- [9] K. M. Kojima, R. Kadono, M. Miyazaki, M. Hiraishi, I. Yamauchi, A. Koda, Y. Tsuchiya, H. S. Suzuki, and H. Kitazawa, Magnetic Frustration in Iridium Spinel Compound CuIr_2S_4 , *Phys. Rev. Lett.* **112**, 087203 (2014).
- [10] Y. F. Nie, P. D. C. King, C. H. Kim, M. Uchida, H. I. Wei, B. D. Faeth, J. P. Ruf, J. P. C. Ruff, L. Xie, X. Pan, C. J. Fennie, D. G. Schlom, and K. M. Shen, Interplay of Spin-Orbit Interactions, Dimensionality, and Octahedral Rotations in Semimetallic SrIrO_3 , *Phys. Rev. Lett.* **114**, 016401 (2015).
- [11] O. B. Korneta, S. Chikara, S. Parkin, L. E. DeLong, P. Schlottmann, and G. Cao, Pressure-induced insulating state in $\text{Ba}_{1-x}\text{R}_x\text{IrO}_3$ ($R = \text{Gd}, \text{Eu}$) single crystals, *Phys. Rev. B* **81**, 045101 (2010).
- [12] M. K. Crawford, M. A. Subramanian, R. L. Harlow, J. A. Fernandez-Baca, Z. R. Wang, and D. C. Johnston, Structural and magnetic studies of Sr_2IrO_4 , *Phys. Rev. B* **49**, 9198 (1994).
- [13] J. Nichols, N. Bray-Ali, A. Ansary, G. Cao, and K.-W. Ng, Tunneling into the Mott insulator Sr_2IrO_4 , *Phys. Rev. B* **89**, 085125 (2014).
- [14] S. Chikara, D. Haskel, J.-H. Sim, H.-S. Kim, C.-C. Chen, G. Fabbri, L. S. I. Veiga, N. M. Souza-Neto, J. Terzic, K. Butrouna, G. Cao, M. J. Han, and M. van Veenendaal, $\text{Sr}_2\text{Ir}_{1-x}\text{Rh}_x\text{O}_4$ ($x < 0.5$): An inhomogeneous $j_{\text{eff}} = 1/2$ Hubbard system, *Phys. Rev. B* **92**, 081114(R) (2015).
- [15] S. Chikara, G. Fabbri, J. Terzic, G. Cao, D. Khomskii, and D. Haskel, Charge partitioning and anomalous hole doping in Rh-doped Sr_2IrO_4 , *Phys. Rev. B* **95**, 060407(R) (2017).

- [16] O. B. Korneta, T. Qi, S. Chikara, S. Parkin, L. E. De Long, P. Schlottmann, and G. Cao, Electron-doped $\text{Sr}_2\text{IrO}_{4-\delta}$; ($0 \leq \delta \leq 0.04$): Evolution of a disordered $J_{\text{eff}} = 1/2$ Mott insulator into an exotic metallic state, *Phys. Rev. B* **82**, 115117 (2010).
- [17] H.-M. Guo and M. Franz, Three-Dimensional Topological Insulators on the Pyrochlore Lattice, *Phys. Rev. Lett.* **103**, 206805 (2009).
- [18] T. Gog, D. M. Casa, A. H. Said, M. H. Upton, J. Kim, I. Kuzmenko, X. Huang, and R. Khachatryan, Spherical analyzers and monochromators for resonant inelastic hard X-ray scattering: A compilation of crystals and reflections, *J. Synchrotron Radiat.* **20**, 74 (2013).
- [19] Yu. V. Shvyd'ko, Merix—next generation medium energy resolution inelastic X-ray scattering instrument at the APS, *J. Electron Spectrosc. Relat. Phenom.* **188**, 140 (2013).
- [20] G. Kresse and J. Furthmüller, Efficient iterative schemes for ab initio total-energy calculations using a plane-wave basis set, *Phys. Rev. B* **54**, 11169 (1996).
- [21] G. Kresse and D. Joubert, From ultrasoft pseudopotentials to the projector augmented-wave method, *Phys. Rev. B* **59**, 1758 (1999).
- [22] J. P. Perdew, B. Kieron, and M. Ernzerhof, Generalized Gradient Approximation Made Simple, *Phys. Rev. Lett.* **77**, 3865 (1996).
- [23] A. C. Larson and R. B. Von Dreele, General Structure Analysis System (GSAS), Los Alamos National Laboratory Report No. LAUR, 86 2004.
- [24] B. H. Toby, EXPGUI, a graphical user interface for GSAS, *J. Appl. Crystallogr.* **34**, 210 (2001).
- [25] A. V. Zakrzewski, S. Gangopadhyay, and G. J. MacDougall, Evolution of magnetic and orbital properties in the magnetically diluted A-site spinel $\text{Cu}_{1-x}\text{Zn}_x\text{Rh}_2\text{O}_4$, *Phys. Rev. B* **97**, 214411 (2018).
- [26] X. Wang, Y. Guo, Y. Shi, A. A. Belik, Y. Tsujimoto, W. Yi, Y. Sun, Y. Shirako, M. Arai, M. Akaogi, Y. Matsushita, and K. Yamaura, High-pressure synthesis, crystal structure, and electromagnetic properties of CdRh_2O_4 : An analogous oxide of the postspinel mineral MgAl_2O_4 , *Inorg. Chem.* **51**, 6868 (2012).
- [27] G. Blasse, Crystal chemistry and some magnetic properties of mixed metal oxides with spinel structure, Philips Research Reports Supplements **3**, 1 (1964).
- [28] S. Zabinsky, J. J. Rehr, A. Ankudinov, R. C. Albers, and M. J. Eller, Multiple-scattering calculations of x-ray-absorption spectra, *Phys. Rev. B* **52**, 2995 (1995).
- [29] M. Grioni, J. F. van Acker, M. T. Czyzyk, and J. C. Fuggle, Unoccupied electronic structure and core-hole effects in the x-ray-absorption spectra of Cu_2O , *Phys. Rev. B* **45**, 3309 (1992).
- [30] D. T. Cromer and D. Liberman, Anomalous dispersion calculations near to and on the long-wavelength side of an absorption Q edge, *Acta Crystallogr.* **A37**, 267 (1981); G. Van der Laan and B. T. Thole, Local Probe for Spin-Orbit Interaction, *Phys. Rev. Lett.* **60**, 1977 (1988).
- [31] J. Stöhr and H. König, Determination of Spin- and Orbital-Moment Anisotropies in Transition Metals by Angle-Dependent X-Ray Magnetic Circular Dichroism, *Phys. Rev. Lett.* **75**, 3748 (1995).
- [32] M. A. Laguna-Marco, D. Haskel, N. Souza-Neto, J. Lang, V. Krishnamurthy, S. Chikara, G. Cao, and M. Veenendaal, Orbital Magnetism and Spin-Orbit Effects in the Electronic Structure of BaIrO_3 , *Phys. Rev. Lett.* **105**, 216407 (2010).
- [33] M. A. Laguna-Marco, P. Kayser, J. A. Alonso, M. J. Martínez-Lope, M. van Veenendaal, Y. Choi, and D. Haskel, Electronic structure, local magnetism, and spin-orbit effects of Ir(IV)-, Ir(V)-, and Ir(VI)-based compounds, *Phys. Rev. B* **91**, 214433 (2015).
- [34] M. Kusch, V. M. Katukuri, N. A. Bogdanov, B. Büchner, T. Dey, D. V. Efremov, J. E. Hamann-Borrero, B. H. Kim, M. Krisch, A. Maljuk, M. Moretti Sala, S. Wurmehl, G. Aslan-Cansever, M. Sturza, L. Hozoi, J. van den Brink, and J. Geck, Observation of heavy spin-orbit excitations propagating in a nonmagnetic background: The case of $(\text{Ba}, \text{Sr})_2\text{YrO}_6$, *Phys. Rev. B* **97**, 064421 (2018).
- [35] A. Nag, S. Bhowal, A. Chakraborty, M. M. Sala, A. Efimenko, F. Bert, P. K. Biswas, A. D. Hillier, M. Itoh, S. D. Kaushik, V. Siruguri, C. Meneghini, I. Dasgupta, and S. Ray, Origin of magnetic moments and presence of spin-orbit singlets in Ba_2YrO_6 , *Phys. Rev. B* **98**, 014431 (2018).
- [36] Y.-J. Kim, J. P. Clancy, H. Gretarsson, G. Cao, Y. Singh, J. Kim, M. H. Upton, D. Casa, and T. Gog, Probing electronic excitations in iridates with resonant inelastic x-ray scattering and emission spectroscopy techniques, [arXiv:1805.03612](https://arxiv.org/abs/1805.03612).
- [37] K. Ishii, I. Jarrige, M. Yoshida, K. Ikeuchi, J. Mizuki, K. Ohashi, T. Takayama, J. Matsuno, and H. Takag, Momentum-resolved electronic excitations in the Mott insulator Sr_2IrO_4 studied by resonant inelastic x-ray scattering, *Phys. Rev. B* **83**, 115121 (2011).
- [38] H. Gretarsson, J. P. Clancy, X. Liu, J. P. Hill, E. Bozin, Y. Singh, S. Manni, P. Gegenwart, J. Kim, A. H. Said, D. Casa, T. Gog, M. H. Upton, H.-S. Kim, J. Yu, V. M. Katukuri, L. Hozoi, J. van den Brink, and Y.-J. Kim, Crystal-Field Splitting and Correlation Effect on the Electronic Structure of A_2IrO_3 , *Phys. Rev. Lett.* **110**, 076402 (2013).
- [39] X. Liu, V. M. Katukuri, L. Hozoi, W.-G. Yin, M. P. M. Dean, M. H. Upton, J. Kim, D. Casa, A. Said, T. Gog, T. F. Qi, G. Cao, A. M. Tselvik, J. van den Brink, and J. P. Hill, Testing the Validity of the Strong Spin-Orbit-Coupling Limit for Octahedrally Coordinated Iridate Compounds in a Model System $\text{Sr}_3\text{CuIrO}_6$, *Phys. Rev. Lett.* **109**, 157401 (2012).
- [40] J. Kim, M. Daghofer, A. H. Said, T. Gog, J. van den Brink, G. Khaliullin, and B. J. Kim, Excitonic quasiparticles in a spin-orbit mott insulator, *Nat. Commun.* **5**, 4453 (2014).
- [41] J. M. Kahn, C. G. Poll, F. E. Oropeza, J. M. Ablett, D. Céolin, J.-P. Rueff, S. Agrestini, Y. Utsumi, K. D. Tsuei, Y. F. Liao, F. Borgatti, G. Panaccione, A. Regoutz, R. G. Egdell, B. J. Morgan, D. O. Scanlon, and D. J. Payne, Understanding the Electronic Structure of IrO_2 using Hard-X-Ray Photoelectron Spectroscopy and Density-Functional Theory, *Phys. Rev. Lett.* **112**, 117601 (2014).
- [42] J. P. Clancy, H. Gretarsson, E. K. H. Lee, D. Tian, J. Kim, M. H. Upton, D. Casa, T. Gog, Z. Islam, B.-G. Jeon, K. H. Kim, S. Desgreniers, Y. B. Kim, S. J. Julian, and Y.-J. Kim, X-ray scattering study of pyrochlore iridates: Crystal structure, electronic, and magnetic excitations, *Phys. Rev. B* **94**, 024408 (2016).

- [43] S. H. Chun, B. Yuan, D. Casa, J. Kim, Chang-Yong Kim, Z. Tian, Y. Qiu, S. Nakatsuji, and Y.-J. Kim, Magnetic Excitations across the Metal-Insulator Transition in the Pyrochlore Iridate $\text{Eu}_2\text{Ir}_2\text{O}_7$, *Phys. Rev. Lett.* **120**, 177203 (2018).
- [44] A. P. Ramirez, G. Lawes, D. Li, and M. A. Subramanian, Valence-electron transfer and a metal-insulator transition in a strongly correlated perovskite oxide, *Solid State Commun.* **131**, 251 (2004).
- [45] F. Sun, H. Zheng, Y. Liu, E. D. Sandoval, C. Xu, J. Xu, C. Q. Jin, C. J. Sun, W. G. Yang, H. K. Mao, J. F. Mitchell, A. N. Kolmogorov, and D. Haskel, Electronic and structural response to pressure in the hyperkagome-lattice $\text{Na}_3\text{Ir}_3\text{O}_8$, *Phys. Rev. B* **98**, 085131 (2018).